Towards artificial photosynthesis on the lipid bilayer of liposomes

Klein, D.M.

Chapter 2

Unidirectional transmembrane photoinduced electron transfer with membrane-embedded metallopeptides

Unidirectional transmembrane electron transfer is an essential process in natural photosynthetic solar energy conversion, where it plays a key role in separating reaction products and slowing charge recombination. Biomimicking photosynthetic membranes by making use of artificial liposomes to demonstrate transmembrane electron transfer is a challenging strategy; in particular, differentiating genuine transmembrane electron transfer through a molecularly impermeable lipid membrane, from light-induced leakage of molecular electron donors or acceptors through the membrane, followed by photoelectron transfer at the surface of the bilayer, is a complicated task. Here, we report two membrane-embedded metallopeptides, ***WALP23-Ru$_2$*** *and* ***WALP23-Re$_2$****, designed to drive photoinduced transmembrane electron transfer in liposomes. Upon light irradiation, the polycationic peptide* ***WALP23-Ru$_2$*** *seemed to quickly transfer electrons from a donor located in a liposome interior, to an acceptor located on the other side of the membrane. However, a membrane leakage assay demonstrated that the reaction was the result of leakage of the electron donor through the membrane, followed by photoinduced electron transfer on one side of the membrane. In contrast, the neutral peptide* ***WALP23-Re$_2$*** *achieved slower light-induced electron transfer, but without leakage, thereby realizing genuine transmembrane electron transfer. These results highlight the importance of leakage studies for the development of biomimicking artificial photosynthetic systems and the potential of artificial metallopeptides as transmembrane electron transporters.*

This chapter is to be submitted as a full paper: David M. Klein, Xinmeng Li, Aimee L. Boyle, Rianne van der Pol, G. J. Agur Sevink, Albert M. Brouwer, and Sylvestre Bonnet, *in preparation*.

2.1 Introduction

In natural photosynthesis, the efficiency of electron extraction from water in green plants is optimised by embedding all key components of the system, i.e. the oxygen evolving complex, photosystem I, and photosystem II, around the lipid bilayer of the photosynthetic membrane. Unidirectional electron transfer through the membrane is achieved using several redox mediators assembled at fixed positions inside the membrane, as well as a tight, evolutionary-evolved Z-like energy scheme, which prevents non-productive charge recombination.[1] This system allows green plants to use the energy from sunlight and catalytic water oxidation to perform CO_2 reduction and produce sugars via the Calvin cycle. A promising strategy for artificial solar fuel production is to mimic natural photosynthesis using the lipid bilayer of liposomes as a platform for the co-embedding of catalysts and photosensitisers.[2–4] Liposomes are spherical supramolecular assemblies of lipids that define two distinct aqueous compartments, i.e., an inner compartment and the exterior bulk aqueous phase, and one lipophilic phase, i.e., the interior of the membrane. These compartments can be exploited for artificial photosynthetic purposes by separating water-soluble components (i.e. electron donors from electron acceptors, or water oxidation catalysts from water reduction catalysts) to avoid energy-wasting charge recombination reactions. To enable electrons running from one compartment to the other, for example to couple water oxidation with water reduction, it is crucial to be able to transfer electrons across the lipid bilayer. The membrane is, however, an insulator, and it is also too thick (typically 30 – 35 Å) for allowing electron transfer to occur in one single step.[4,5]

Driving unidirectional photoinduced electron transfer through an insulating lipid membrane is hence recognised as one of the holy grails of artificial photosynthesis. Three main strategies have been considered to achieve it: 1) incorporation of biological components, such as an electron-transfer transmembrane protein, into the lipid bilayer[6,7]; 2) synthesis of artificial transmembrane molecules spanning the lipid bilayer[8–10]; and 3) use of molecular charge carriers that can diffuse across the membrane[11]. Still, the

number of liposomal systems that can actually perform transmembrane electron transfer is limited.[6–11] These strategies indeed share many challenges, such as difficult syntheses, problems in controlling the orientation of a dissymmetric molecule relative to a lipid bilayer separating two different aqueous environments, or quenching of the photoinduced electron transfer reaction in the presence of molecular dioxygen. In addition, the mechanistic problem of distinguishing the leakage of redox mediator molecules through the membrane, followed by electron transfer on one side of the membrane, from genuine transmembrane electron transfer across a truly impermeable bilayer, has rarely been discussed.[2,12,13]

To address these challenges simultaneously, we prepared two new metallopeptides, **WALP23-Ru_2** and **WALP23-Re_2**, which are well-defined, air-stable molecules designed to place two identical ruthenium(II) or rhenium(I) photosensitisers at intermediate positions inside a lipid bilayer membrane. Ideally, such a molecule may allow transmembrane electron transfer to occur in three shorter (< 20 Å) steps, rather than one large step of more than 40 Å, which is highly improbable.[5] We investigated the orientation of the metallopeptides within the membrane and their ability to transfer electrons, upon light irradiation, across a lipid bilayer, from an electron donor located in the inner compartment of the liposome, towards an electron acceptor located outside, i.e., in the bulk (Figure 2.1A, pathway I). By using a membrane leakage assay, we were able to distinguish genuine transmembrane electron transfer, which takes place with **WALP23-Re_2**, from transmembrane leakage of the electron donor, which occurs with **WALP23-Ru_2** (Figure 2.1A, pathway II).

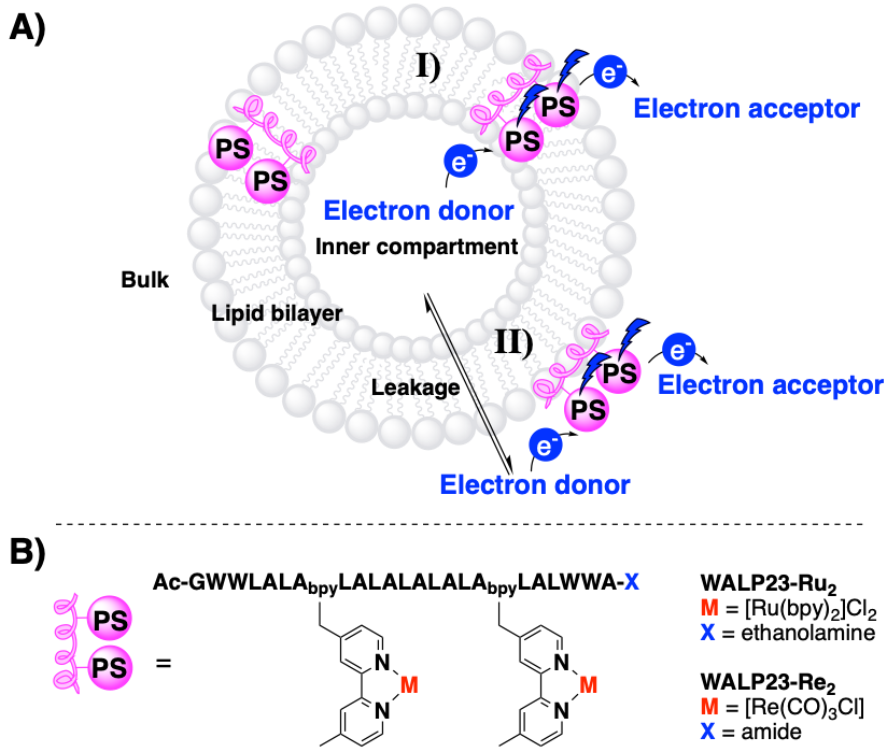

Figure 2.1. Transmembrane electron transfer with metallopeptides in the lipid bilayer. (**A**) Two pathways for electron transfer are possible; I) electron transfer across the lipid bilayer via a light-activatable metallopeptide from an electron donor in the inner compartment of liposomes to an electron acceptor located in the aqueous bulk, and II) transmembrane leakage of the electron donor to the aqueous bulk resulting in electron transfer via a light-activatable metallopeptide on the same side of the membrane. (**B**) Molecular structure of the metallopeptides investigated in this study. A = alanine, A_{bpy} = bipyridylalanine, Ac = acetyl, G = glycine, L = leucine, and W = tryptophan.

2.2 Results and Discussion

The molecular structure of the metallopeptides **WALP23-Ru$_2$** and **WALP23-Re$_2$** (Figure 2.1B) derives from the WALPn peptides (Ac-GWWL(AL)$_n$WWA-X, with Ac = acetyl, G = glycine, W = tryptophan, L = leucine, A = alanine, and X = amide or ethanolamine). WALPn peptides are hydrophobic α-helical peptides, initially developed by Killian *et al.* as a model for the hydrophobic domains of many transmembrane proteins found in nature.[14–16] We

envisioned that by incorporating at least two metal centers within the peptide chain of WALPn, photoinduced electron transfer may be achieved by splitting it into several steps; 1) light absorption by the photosensitisers resulting in the formation of an excited state PS^*, 2) reductive quenching of PS^* by the electron donor located near the inner compartment of the liposome, resulting in the formation of reduced photosensitiser (PS^-), 3) oxidative quenching of PS^* by the electron acceptor located near the bulk aqueous phase, resulting in the formation of oxidised photosensitiser (PS^+), and finally 4) charge recombination between PS^- and PS^+ within the membrane, to regenerate the two ground state photosensitisers. Thus, we replaced two alanine residues in the original WALPn peptide sequence by two unnatural amino acids that can chelate metal ions, namely bipyridylalanines (A_{bpy}).[17,18] Two parameters of the peptide were designed simultaneously: 1) the length of the α-helical part of the peptide (i.e. the amino acids $L(AL)_n$, where the length of one amino acid is assumed to be 0.15 nm in an ideal α-helix) should fit the hydrophobic thickness of the membrane bilayer (2.65 nm for 1,2-dipalmitoyl-*sn*-glycero-3-phosphocholine; DPPC)[15]; 2) the distance between the two metal centers should be short enough to allow electron transfer between them to occur; ideally both PS molecules should be on the same side of the α-helix. Based on initial modeling using the YASARA program, we chose to prepare a WALP23 peptide (thus Ac-GWWL$(AL)_4$WWA-X) with A_{bpy} residues in positions 7 and 17; **WALP23-bpy$_2$** (Figure B1 and Table B1). We prepared **WALP23-bpy$_2$** by a combination of automated solid-phase peptide synthesis, with manual peptide synthesis for the coupling of the two A_{bpy} residues. The metallopeptides **WALP23-Ru$_2$** and **WALP23-Re$_2$** were then synthesised by reaction of **WALP23-bpy$_2$** with *cis*-$[Ru(bpy)_2Cl_2]$ and $[Re(CO_5)Cl]$ metal precursors, respectively. The metallopeptides were purified by size-exclusion chromatography and characterised by elemental analysis, HPLC-MS (Figures B2 – B4), and UV-Vis (Figures B5 and B6).

Although both metallopeptides were prepared from the same hydrophobic peptide and hence may seem similar, **WALP23-Ru$_2$** bears 4 positive charges and 4 chloride counter anions, while **WALP23-Re$_2$** is neutral. Such different charges are likely to affect the lipophilicity of the peptides, which may in turn

influence their membrane embedding, shape, and/or orientation with respect to the membrane. Molecular dynamics (MD) simulations were performed to study these questions and qualitatively assess whether **WALP23-Ru$_2$** and **WALP23-Re$_2$** may retain the reported propensity of WALP23 to insert into the membrane with a perpendicular orientation with respect to the lipid bilayer. The primary goal of the modeling was to investigate the insertion probability of each peptide. 200 ns MD simulations were hence performed by spontaneous aggregation of independent random mixtures containing one metallopeptide molecule, 128 DPPC lipid molecules solvated by water molecules, and in the case of **WALP23-Ru$_2$**, 4 chloride anions to neutralise the charge of the system. We opted for spontaneous aggregation of the lipid bilayer because the high free energy barrier associated with inserting peptides into a readily formed membrane is known to hamper the observation of spontaneous insertion on the time scales of standard MD.[19–22] The alternative approach, i.e., the determination of a free energy difference by constrained MD[23], suffers from a lack of clearly defined reaction coordinates, as the propensity of the metal centers for the interface is likely to induce important conformational changes in the WALP23 backbone. Earlier studies have also corroborated that, while the kinetics of insertion may vary with particular force field parameters and simulation techniques, the energetics of partitioning can be reliably extracted by different approaches. We note that, whereas NMR data support an insertion motif for WALP23 of an (antiparallel) dimer[24], the (charged) metallic groups at the peptide interface are likely to oppose dimer formation, so only monomers were simulated.

Simulation trajectories were analysed to determine the insertion characteristics of the metallopeptide via its orientational angle (ϑ) and immersion ratio (φ), see Figure 2.2A. Here, ϑ, is defined as the angle between the two metals and the local normal of the lipid membrane, while φ is the ratio between the number of DPPC molecules and the total number of molecules (DPPC, water, and ions) that surround the metallopeptide (within a pre-defined cut-off range of 0.35 nm). Typically, a metallopeptide that would show $\vartheta < 50$ ° and $\varphi > 0.5$ could be considered as “transmembrane”, while metallopeptides with $\vartheta > 50$ ° and $\varphi > 0.5$ could be considered as

"parallel" to the membrane, typically placed at the water-bilayer interface. In the case of $\varphi < 0.5$, the metallopeptide is surrounded by more water molecules than DPPC molecules, and therefore its orientation with respect to the lipid bilayer was not determined. Furthermore, the mass density profiles of the metallopeptides within the lipid bilayer were analysed to verify whether the configuration was truly transmembrane or parallel (Figures B7, B8, and B9). Figure 2.2B shows that in a majority of the cases, a relatively short 200 ns trajectory was sufficient for the metallopeptide to either bind to or insert into a well-identified lipid bilayer membrane, in agreement with the hydrophobic nature of their WALP23 core. While most peptides were found to bind to the membrane, 2 of the 13 simulated **WALP23-Ru_2** peptides led to transmembrane configurations, while for the more hydrophobic **WALP23-Re_2** peptide the number of transmembrane configurations was significantly higher (5 out of 16, as one **WALP23-Re_2** peptide considered as parallel ($\varphi = 0.58$ and $\vartheta = 60$ °) turned out to be in a transmembrane configuration by its mass density profile), see Figures 2.2C and 2.2D. Within the transmembrane configurations, the average distance between the two metal atoms was found to be 2.0 ± 0.3 nm for Ru-Ru and 2.1 ± 0.6 nm for Re-Re (Table B2), which should in theory accommodate electron transfer between them, as electron transfer within biological systems are reported up to 3.5 nm.[5] Importantly, these results highlight that even when designed to assemble perpendicularly to a lipid bilayer membrane, artificial amphipathic molecules may also assemble in a parallel fashion at the interface with water, as such assembly also offers improved molecular contacts with both hydrophobic and hydrophilic phases.

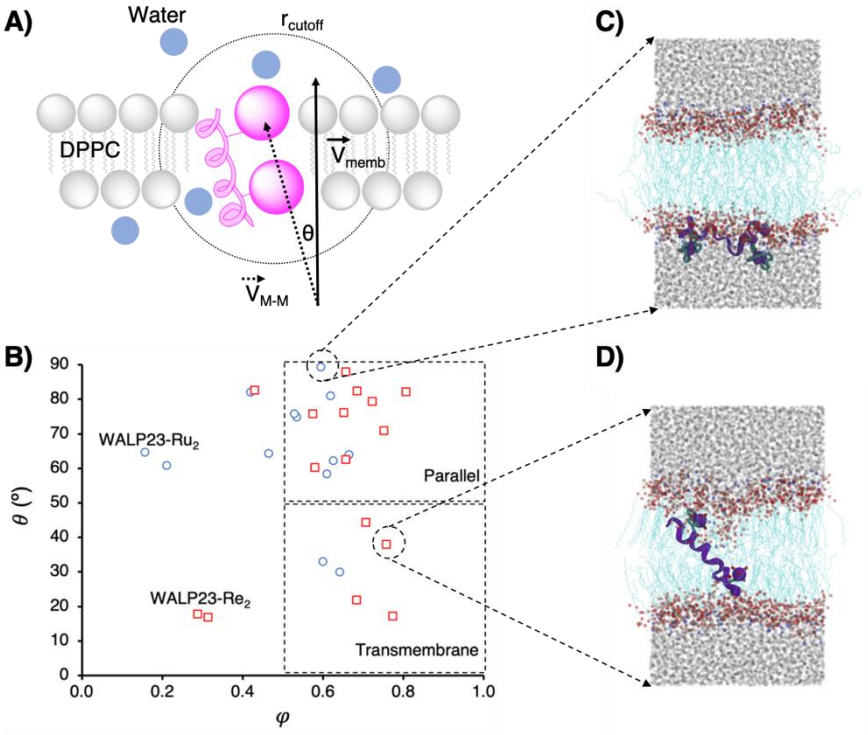

Figure 2.2. Molecular dynamics simulations to study the orientation of the metallopeptides. **(A)** Illustration of the procedure that was used to determine the orientation of the metallopeptide with respect to the lipid membrane. ϑ is the angle between the metal-metal vector ($\vec{V}_{M\text{-}M}$) and the normal vector of the lipid membrane ($\vec{V}_{memb}$). r_{cutoff} is the cut-off range. (**B**) φ and ϑ values of **WALP23-Ru$_2$** and **WALP23-Re$_2$** after 200 ns MD simulation time. φ is the ratio between the number of DPPC molecules and the total number of molecules within r_{cutoff}. (**C**) MD snapshots showing a parallel orientation of **WALP23-Ru$_2$** with respect to the lipid bilayer and (**D**) a transmembrane **WALP23-Re$_2$**.

To determine whether the MD simulations reflect the experimental incorporation of metallopeptides into a DPPC membrane, we prepared metallopeptide-functionalised liposomes. For the preparation of these liposomes, either **WALP23-bpy$_2$, WALP23-Ru$_2$** or **WALP23-Re$_2$** (1 mol%) was added to a DPPC formulation containing one percent 1,2-distearoyl-*sn*-glycero-3-phosphoethanolamine N-(carbonyl-methoxypolyethylene glycol-2000) (NaDSPE-PEG2K), which served to prevent liposome aggregation.[25] The liposomes were prepared by standard extrusion methods using an NH_4OAc

buffer at a pH of 7.0 and an osmolality of 0.42 Osm (see Appendix B). According to dynamic light scattering the average hydrodynamic diameter of the resulting liposomes was 137 nm for liposomes containing **WALP23-bpy$_2$**, 136 nm for liposomes containing **WALP23-Ru$_2$** and 123 nm for liposomes containing **WALP23-Re$_2$**, and their polydispersity index (PDI) was lower than 0.20, which indicated a uniform size distribution (Table B3). As absorption spectra obtained using UV-Vis spectroscopy suffered from strong scattering due to the presence of the liposomes, photoluminescence excitation and emission spectra were measured to characterise the lowest energy absorption (λ_{abs}) and emission maxima (λ_{em}) of the metallopeptides in the liposome environment. λ_{abs} and λ_{em} were 454 nm and 616 nm, respectively, for **WALP23-Ru$_2$**, and 366 nm and 562 nm, respectively, for **WALP23-Re$_2$**, which fits with values typically reported for $[Ru(bpy)_3]^{2+}$ and $[Re(bpy)(CO)_3Cl]$ complexes in lipid membranes (Figure B10).[26,27] For both metallopeptides, emission from the W amino acids (λ_{em} = 334 nm for **WALP23-Ru$_2$** and 335 nm for **WALP23-**Re_2, was slightly blue-shifted compared to **WALP23-bpy$_2$** (λ_{em} = 349 nm, Figure B11). Time-dependent photoluminescence could be best fitted with biexponential decay rate laws, with lifetimes τ_1 = 123 ns and τ_2 = 787 ns for **WALP23-Ru$_2$** and τ_1 = 8 ns and τ_2 = 103 ns for **WALP23-Re$_2$** (Figure B12). Altogether, and also considering that both metallopeptides are insoluble in water, these results strongly indicate that **WALP23-Ru$_2$** and **WALP23-Re$_2$** were indeed taken up by the membrane of the liposomes. This assumption was confirmed using confocal microscopy of the **WALP23-Ru$_2$**-containing multilamellar giant vesicles obtained before extrusion during liposome preparation, which showed red emission (λ_{exc} = 488 nm and λ_{em} = 640 – 680 nm) coming from the lipid bilayer only (Figure B13).

To perform the transmembrane electron transfer experiments, dissymmetric DPPC:NaDSPE-PEG2K (100:1) liposomes were prepared containing 1 mol% of the metallopeptide in the membrane, the electron donor ethylenediaminetetraacetic acid (EDTA; in the form of $HEDTA^{3-}$ at pH = 8.2) in the aqueous inner compartment of the liposome, and the electron acceptor 2-(4-iodophenyl)-3-(4-nitrophenyl)-5-(2,4-disulfophenyl)-2*H*-tetrazolium anion ($WST1^-$) in the bulk aqueous phase, thus on the outside

(pH = 7.0) of the liposome (Figure 2.3). We chose $WST1^-$ as the electron acceptor as lipid membranes are notoriously impermeable to it; this dye is known by biologists to be reduced to formazan ($Fz1^{2-}$) by electrons and protons generated inside living cells only in the presence of a membrane-soluble relay such as the 1-methoxy-*N*-methylphenazinium cation (MMP^+).[11,28] When left in the dark for 30 min, the liposomes were stable and did not show any sign of formazan formation. However, upon light irradiation a new absorption band at λ_{max} = 438 nm gradually appeared that is characteristic of $Fz1^{2-}$ (Figure 2.3).[11] This evolution clearly demonstrated that photoinduced electron transfer had taken place, with a quantum yield of 0.015% for **WALP23-Ru$_2$** and 0.027% for **WALP23-Re$_2$** after 1 h of irradiation (see Appendix B for the calculation and Figure B14). Furthermore, the liposome systems were photoactive under both a N_2 atmosphere and an air atmosphere (Figures B15 – B18), which is a significant improvement over systems requiring MMP^+ as a transmembrane electron transporter for example, which is re-oxidised in the presence of dioxygen.[11] Dynamic light scattering measurements showed that the liposomes remained intact during the photoreaction, as the size and polydispersity remained identical before and after 2.5 h light irradiation (Table B4). A control experiment with **WALP23-bpy$_2$** in the membrane instead of a metallopeptide showed no photoinduced electron transfer, demonstrating that the metal-based photosensitisers were required for light-driven electron transfer (Figure B19). Overall, both membrane-embedded metallopeptides clearly allowed photoinduced electron transfer to occur between the $HEDTA^{3-}$ donor and $WST1^-$ acceptor originally located on opposite sides of the membrane.

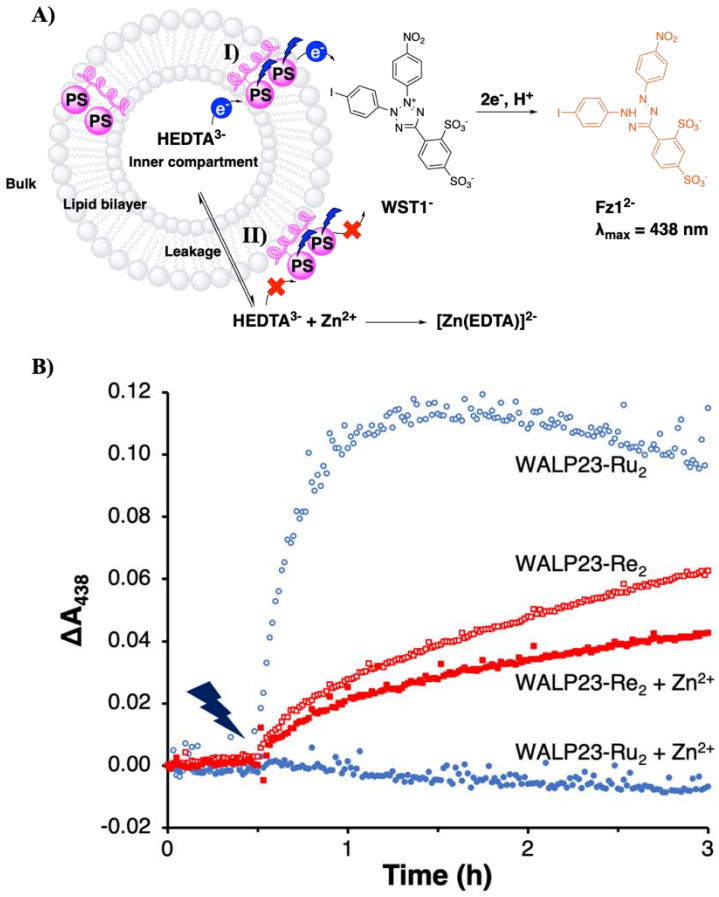

Figure 2.3. Electron transfer studies of the metallopeptides in liposomes. (**A**) Electron transfer processes initiated by light irradiation; I) transmembrane electron transfer from the sacrificial electron donor $HEDTA^{3-}$ located in the inner compartment of the liposome via a membrane-embedded peptide-photosensitiser conjugate to the sacrificial electron acceptor $WST1^{-}$ located in the bulk forming the colored $Fz1^{2-}$, which can be followed by UV-Vis, and II) externally added Zn^{2+} ions form a complex with $HEDTA^{3-}$, thereby inactivating the electron transfer pathway on the outside of the membrane; (**B**) The formation of Fz^{2-} as monitored by a change in absorbance (λ_{max} = 438 nm) versus irradiation time for liposome systems containing either **WALP23-Ru$_2$** (blue circles) or **WALP23-Re$_2$** (red squares) with (closed symbols) or without $Zn(OAc)_2$ (open symbols). Blue light irradiation (λ_{irr} = 450 nm, P = 15.8 mW, Φ_0 = 39.1 nmol/s for **WALP23-Ru$_2$** and λ_{irr} = 385 nm, P = 7.3 mW, Φ_0 = 13.1 nmol/s for **WALP23-Re$_2$**) was started after 0.5 h in the dark. Experimental conditions: [DPPC] = 2.5 mM, [DSPE-PEG2K] = 25 µM, [**WALP23-Ru$_2$** or **WALP23-Re$_2$**] = 25 µM, [$HEDTA^{3-}$] = 0.125 M (before SEC column), [$WST1^{-}$] = 0.33 mM, [$Zn(OAc)_2$] = 0 or 5 mM in 0.1 M NH_4OAc (pH = 7.0, p = 0.42 Osm). The measurements were performed at 25 °C under an air atmosphere.

At this stage, however, it became essential to distinguish unambiguously between genuine transmembrane electron transfer, and leakage of the donor through the membrane, followed by photoinduced electron transfer on one side of the membrane (Figure 2.3A). In order to distinguish between these two mechanisms, an excess of Zn^{2+} ions was added on the outside of the liposomes before light irradiation, keeping the same osmolality as the inner solution using NH_4OAc. Zn^{2+} ions chemically bind to $HEDTA^{3-}$ molecules to form the complex $[Zn(EDTA)]^{2-}$. By doing so, the electron donor ability of $HEDTA^{3-}$ molecules that may have remained outside the liposomes after liposome purification, or that may have leaked through the membrane during the photoreaction, is inactivated.[11] Hence, addition of Zn^{2+} enables the differentiation of true transmembrane electron transfer by excitation of the transmembrane metallopeptide, from leakage of $HEDTA^{3-}$ through the membrane followed by photoinduced electron transfer to $WST1^{-}$ on the outside of the membrane. For liposomes containing the **WALP23-Ru$_2$** metallopeptide the photoinduced electron transfer observed in the absence of Zn^{2+} ions was fully quenched when Zn^{2+} was added, while those containing **WALP23-Re$_2$** conserved their ability to transfer electrons (at a slightly lower rate, Figure 2.3B). Additional control experiments were realised using mononuclear photosensitisers $[Ru(bpy)_2(bpy\text{-}(C_{15})_2)]Cl_2$ (bpy = 2,2'-bipyridine; bpy-$(C_{15})_2$ = 4,4'-di-pentadecane-2,2'-bipyridine) or $[Re(bpy\text{-}(C_{15})(CO)_3Cl]$ instead of the metallopeptides, which distribute on both leaflets of the bilayer and are not physically coupled to each other as in **WALP23-Ru$_2$** or **WALP23-Re$_2$** (Figures B20 and B21).[27] All other conditions being identical, these experiments showed much slower electron transfer compared to membranes functionalised with the metallopeptides, which were deactivated upon addition of free Zn^{2+} ions on the outside of the liposomes (Figure B22). These controls demonstrate that the mechanical link and close distance between the two metals in the metallopeptide play a crucial role in their transmembrane electron transfer abilities.

To investigate in more detail why **WALP23-Ru$_2$** showed formation of $Fz1^{2-}$ in absence of Zn^{2+} ions, while it was unable to do so in the presence of Zn^{2+} ions, whereas electron transfer with **WALP23-Re$_2$** was more or less insensitive to zinc addition, we quantified $HEDTA^{3-}$ leakage through the membrane using a

murexide-based titration experiment.[11] Murexide is a purple dye that becomes orange upon binding to Cu^{2+}, but cannot compete with copper chelation by $HEDTA^{3-}$. Addition of an excess of murexide to liposomes kept in the dark or irradiated with light, followed by dropwise titration with known amounts of Cu^{2+}, allowed the quantification of the amount of $HEDTA^{3-}$ in the outside aqueous phase (Table B5). The concentration of $HEDTA^{3-}$ outside the liposomes was found to be low (0.0 – 0.2 mM) for liposomes containing either **WALP23-Ru$_2$** or **WALP23-Re$_2$** metallopeptides. This result indicated that i) purification of the asymmetric liposomes using size-exclusion chromatography was successful at removing $HEDTA^{3-}$ located on the outside of the liposomes, and ii) leakage of $HEDTA^{3-}$ through the membrane did not occur in the dark. In contrast, for irradiated liposomes containing **WALP23-Ru$_2$** in the membrane, the amount of $HEDTA^{3-}$ outside the liposomes increased significantly (from 0.0 – 0.2 mM to 0.2 – 0.4 mM) upon irradiation. Similar results were obtained upon irradiation of liposomes containing **WALP23-Re$_2$** in the membrane (from 0.0 – 0.2 mM to 0.4 – 0.6 mM $HEDTA^{3-}$ outside the liposomes). In both cases, the amount of $HEDTA^{3-}$ was much smaller than the amount of Zn^{2+} ions (5 mM) present, thus all $HEDTA^{3-}$ molecules located on the outside of the liposomes were inactivated as electron donors. Considering that with **WALP23-Ru$_2$** photoinduced electron transfer was fully inactivated in the presence of Zn^{2+} ions, the photoinduced electron transfer occurring in absence of Zn^{2+} ions can essentially be attributed to light-induced leakage of $HEDTA^{3-}$, followed by photosensitised electron transfer at the liposome surface from donor to acceptor molecules both located outside the liposomes. It is likely that such a process is sensitised *via* **WALP23-Ru$_2$** molecules assembled parallel to the lipid membrane. Another hypothesis is that light-induced leakage of Zn^{2+} from the bulk to the inner compartment of the liposomes resulted in the inactivation of the inner $HEDTA^{3-}$ molecules. In contrast, for **WALP23-Re$_2$** electron transfer still occurred after addition of Zn^{2+} ions, which could only take place from $HEDTA^{3-}$ molecules protected from Zn^{2+} ions, hence inside the liposomes, towards $WST1^{-}$ outside the liposomes. Control liposomes containing mononuclear photosensitisers ($[Ru(bpy)_2(bpy\text{-}(C_{15})_2)]Cl_2$ or $[Re(bpy\text{-}(C_{15})(CO)_3Cl]$) showed, both in the dark and after light irradiation, the same concentration of $HEDTA^{3-}$ (0.4 – 0.6 mM) outside the liposomes. It was

hence photoinduced electron transfer on one side of the membrane that occurred for these liposomes, rather than transmembrane photoinduced electron transfer, which again highlights the importance of the mechanical link between the two metal centers in the metallopeptides to trigger true transmembrane electron transfer. Overall, **WALP23-Re$_2$** is one of the few known artificial molecules capable of triggering true transmembrane electron transfer.

2.3 Conclusion

To conclude, metallopeptides built by attaching two neutral rhenium(I) photosensitiser molecules on a WALP23 peptide are capable of performing unidirectional transmembrane electron transfer under an air atmosphere. In such studies, careful examination of the concentration of the encapsulated electron donor, both before and after light irradiation, and both inside and outside the membrane, is crucial to differentiate genuine transmembrane electron transfer, as obtained with **WALP23-Re$_2$**, from light-induced leakage of the electron donor, as observed with **WALP23-Ru$_2$**. In addition, the high modularity of solid-state peptide synthesis allows for imagining a range of metallopeptides with different lengths, and different numbers and relative positions of the metal centers in the membrane, which may lead to optimised transmembrane electron transfer rates without a need for major variations in the synthetic procedure of the "wire". Ultimately, a better fundamental understanding of these systems will be required before fully artificial photosynthetic systems can be developed, where biomimetic transmembrane electron transfer allows for coupling catalytic water oxidation and proton or CO_2 reduction.

2.4 References

1 D. Gust and T.A. Moore, *Science*, 1989, **244**, 35–41.
2 J. N. Robinson and D. J. Cole-Hamilton, *Chem. Soc. Rev.*, 1991, **20**, 49–94.
3 M. Hansen, S. Troppmann and B. König, *Chem. Eur. J.*, 2016, **22**, 58–72.
4 A. Pannwitz, D. M. Klein, S. Rodríguez-Jiménez, C. Casadevall, H. Song, E.

Reisner, L. Hammarström and S. Bonnet, *Chem. Soc. Rev.*, 2021, **50**, 4833–4855.
5 C. C. Moser, J. M. Keske, K. Warncke, R. S. Farid and P. L. Dutton, *Nature*, 1992, **355**, 796–802.
6 E. Altamura, F. Milano, R. R. Tangorra, M. Trotta, O. H. Omar, P. Stano and F. Mavelli, *Proc. Natl. Acad. Sci. U. S. A.*, 2017, **114**, 3837–3842.
7 A. Stikane, E. T. Hwang, E. V. Ainsworth, S. E. H. Piper, K. Critchley, J. N. Butt, E. Reisner and L. J. C. Jeuken, *Faraday Discuss.*, 2019, **215**, 26–38.
8 G. Steinberg-Yfrach, P. A. Liddell, S.-C. Hung, A. L. Moore, D. Gust and T. A. Moore, *Nature*, 1997, **385**, 239–241.
9 S. Bhosale, A. L. Sisson, P. Talukdar, A. Fürstenberg, N. Banetji, E. Vauthey, G. Bollot, J. Mareda, C. Röger, F. Würthner, N. Sakai and S. Matile, *Science*, 2006, **313**, 84–86.
10 A. Perez-Velasco, V. Gorteau and S. Matile, *Angew. Chem. Int. Ed.*, 2008, **47**, 921–923.
11 B. Limburg, E. Bouwman and S. Bonnet, *Chem. Commun.*, 2015, **51**, 17128–17131.
12 L. Hammarström, M. Almgren, J. Lind, G. Merenyi, T. Norrby and B. Åkermark, *J. Phys. Chem.*, 1993, **97**, 10083–10091.
13 L. Hammarström and M. Almgren, *J. Chem. Sci.*, 1993, **105**, 539–554.
14 J. A. Killian, I. Salemink, M. R. R. de Planque, G. Lindblom, R. E. Koeppe and D. V Greathouse, *Biochemistry*, 1996, **35**, 1037–1045.
15 M. R. R. de Planque and J. A. Killian, *Mol. Membr. Biol.*, 2003, **20**, 271–284.
16 J. A. Killian and T. K. M. Nyholm, *Curr. Opin. Struct. Biol.*, 2006, **16**, 473–479.
17 K. J. Kise and B. E. Bowler, *Inorg. Chem.*, 2002, **41**, 379–386.
18 I. Gamba, I. Salvadó, G. Rama, M. Bertazzon, M. I. Sánchez, V. M. Sánchez-Pedregal, J. Martínez-Costas, R. F. Brissos, P. Gamez, J. L. Mascareñas, M. Vázquez López and M. E. Vázquez, *Chem. Eur. J.*, 2013, **19**, 13369–13375.
19 S. Esteban-Martín and J. Salgado, *Biophys. J.*, 2007, **92**, 903–912.
20 J. P. Ulmschneider, J. C. Smith, S. H. White and M. B. Ulmschneider, *J. Am. Chem. Soc.*, 2011, **133**, 15487–15495.
21 T. Bereau, W. F. D. Bennett, J. Pfaendtner, M. Deserno and M. Karttunen, *J. Chem. Phys.*, 2015, **143**, 243127.
22 I. Kabelka and R. Vácha, *Biophys. J.*, 2018, **115**, 1045–1054.
23 T. Kim and W. Im, *Biophys. J.*, 2010, **99**, 175–183.
24 L. Monticelli, D. P. Tieleman and P. F. J. Fuchs, *Biophys. J.*, 2010, **99**, 1455–1464.
25 B. Limburg, J. Wermink, S. S. van Nielen, R. Kortlever, M. T. M. Koper, E. Bouwman and S. Bonnet, *ACS Catal.*, 2016, **6**, 5968–5977.
26 N. Ikuta, S. Y. Takizawa and S. Murata, *Photochem. Photobiol. Sci.*, 2014, **13**, 691–702.
27 D. M. Klein, S. Rodríguez-Jiménez, M. E. Hoefnagel, A. Pannwitz, A. Prabhakaran, M. A. Siegler, T. E. Keyes, E. Reisner, A. M. Brouwer and S. Bonnet, *Chem. Eur. J.*, 2021, **27**, 17203–17212.

28 M. Ishiyama, M. Shiga, K. Sasamoto, M. Mizoguchi and P. He, *Chem. Pharm. Bull.*, 1993, **41**, 1118–1122.